Optimization of Aptamer-Based Electrochemical Biosensor for ATP Detection Using Screen-Printed Carbon Electrode/Gold Nanoparticles (SPCE/AuNP)

Rahmaniar Mulyani[1,2], Nida Yumna[1], Iman Permana Maksum[1], Toto Subroto[1], and Yeni Wahyuni Hartati[1*]**

[1]*Department of Chemistry, Faculty of Mathematics and Natural Sciences, Universitas Padjadjaran, Jl. Raya Bandung-Sumedang Km. 21, Jatinangor 45363, West Java, Indonesia*

[2]*Department of Chemistry, Faculty of Sciences and Informatics, Universitas Jenderal Achmad Yani, Jl. Terusan Jenderal Sudirman, Cimahi 40531, West Java, Indonesia*

* ***Corresponding author:***

tel: +62-8122132349;*
*+62-82240839482***
email: yeni.w.hartati@unpad.ac.id;*
*iman.permana@unpad.ac.id***

Received: February 5, 2022
Accepted: June 16, 2022

DOI: 10.22146/ijc.72820

Abstract: *Electrochemical biosensors are used to detect adenosine triphosphate (ATP) levels, which are involved in a variety of biological processes, such as regulating cellular metabolism and biochemical pathways. Therefore, this research aims to develop an aptamer-based electrochemical biosensor with Screen Printed Carbon Electrode/gold nanoparticles (SPCE/AuNP) and collect data as well as information related to ATP detection. The modification of SPCE with AuNP increased the analyte's binding sensitivity and biocompatibility. The aptamer was selected based on its excellent bioreceptor characteristics. Furthermore, aptamer–SH (F1) and aptamer-NH_2 (F2) were immobilized on the SPCE/AuNP surface, which had been characterized using SEM, EIS, and DPV. Also, the ATP-binding aptamers were electrochemically characterized using the $K_3[Fe(CN)_6]$ redox system and Differential Pulse Voltammetry (DPV). According to the optimization results using the Box-Behnken experimental design, the ideal conditions obtained from the factors influencing the experiment were the F1 concentration and incubation time of 4 μM and 24 h, respectively, as well as F1/F2/ATP incubation time of 7.5 min. Meanwhile, for the range of 0.1 to 100 μM, the detection (LoD) and quantification (LoQ) limits were 7.43 and 24.78 μM, respectively. Therefore, this aptasensor method can be used to measure ATP levels in real samples.*

Keywords: *adenosine triphosphate (ATP); aptamer; AuNP; electrochemistry; screen printed carbon electrode (SPCE)*

■ INTRODUCTION

Adenosine triphosphate (ATP) plays an essential role in many biological processes, such as regulating cellular metabolism and biochemical pathways [1]. Most mitochondrial diseases arise due to disturbances in the process of oxidative phosphorylation. When this process is inhibited, the important role of mitochondria in producing energy in the form of ATP is disrupted, resulting in cellular abnormalities and cell death [2].

Previous research studies have shown that diabetes mellitus and cataracts are caused by mutations that occur in the respiratory complex [3-4]. The prospect that the development of aptasensor application diagnostic methods for diagnosing mitochondrial diabetes can strengthen previous research that has studied mitochondrial DNA mutation studies both *in vitro* and *in silico* [5-7].

The function of biological ATP in biochemical studies, clinical diagnosis, and environmental analysis are essential, necessitating the development of sensitive and specific methods for its recognition and detection. Various techniques, such as fluorometric methods [8-10], high-performance liquid chromatography (HPLC) [11], mass spectrometry [12], chemiluminescence [13], and electrochemistry [14] have been used to detect ATP. However, electrochemical sensors attract more attention

due to their advantages in sensitivity, miniaturization ability, minimal power requirements, low cost, and high stability [15].

An electrochemical biosensor is an integrated receptor-transducer analytical device based on a biologically identifiable element in combination or in close contact with an electrochemical transducer [16]. The measurement is based on the observation of an active reaction that produces a measurable current, potential changes, or impedance resulting from a change in conductance, which is read using voltammetric, amperometric, potentiometric, or impedance methods [17].

The electrochemical biosensor developed in this research uses aptamer bioreceptors, also known as aptasensors. Furthermore, aptamers are short pieces of single-stranded DNA molecules that recognize specific target molecules. It was selected based on its characteristics as bioreceptors, some of which are similar to or even better than antibodies. Therefore, it generates an excellent affinity for biosensors and other applications, such as biomedical imaging, targeted drug delivery, and biomarker discovery [18].

Aptasensors, due to their advantages, have been widely used to detect ATP. For example, Mashhadizadeh et al. developed an electrochemical aptasensor for ATP with a non-enzymatic strategy using graphene oxide-modified silver nanoparticles with a detection limit of 5 nM [19]. Furthermore, Zheng et al. developed an electrochemical nanoaptasensor to monitor the continuous fluctuations of ATP at the subcellular level with a detection limit of 26 μM [20].

Aptamers were immobilized on the electrode surface for biosensor construction. Meanwhile, several aptasensor devices were developed using the Screen-Printed Carbon Electrode (SPCE), which combines a carbon working, reference, and a support electrode in one simple and easy-to-use design [21-22]. SPCE is widely used because of its small size, ease of mass production, low cost, ability to improve electrochemical performance, and ease of modification [23-24].

Modifications were made using gold nanoparticles to increase the sensitivity and conductivity of the analyte signal. Also, due to the large effective surface area and high electrocatalytic ability, gold nanoparticles (AuNP) have been widely used to modify electrode surfaces [25].

Gold nanoparticles have a high surface area, can improve the stability and immobilization of bioreceptors, and function as electron transfer between the bioreceptors and the electrode surface to produce significant signal amplification [26]. These nanoparticles, which are used as signal amplification elements, have received much attention due to their ease of synthesis, unique size, shape, and optical properties, as well as good biocompatibility [27]. Therefore, this research aims to develop an aptamer-based electrochemical biosensor with SPCE/AuNP and collect data as well as information related to the detection of ATP.

■ EXPERIMENTAL SECTION

Materials

The materials used in this study include aqua pro injection (PT Ikapharmindo Putramas), gold nanoparticles (AuNP) synthesized by the citrate reduction method at the Research Center for Biotechnology and Bioinformatics, Universitas Padjadjaran, magnesium chloride 2.0 M, sodium hydroxide 0.1 M, hydrochloric acid 0.1 M, potassium chloride 0.1 M (Merck), tris-(2 carboxyethyl) phosphine hydrochloride 0.5 mM (TCEP) (Sigma), phosphate-buffered saline pH 7.0 (PBS) (Merck), $K_3(Fe[CN]_6)$ 10 mM (Sigma), ATP 100 mM, CTP 100 mM, GTP 100 mM, UTP 100 mM (Roche Diagnostic GmbH), and amino-labeled oligonucleotides and thiol-labeled oligonucleotides (Bioneer) in the following orde': F1: 5'-HS-$(CH_2)_6$-ACCTGGGG'AGTAT-3' and F2: 5'-TGCGGAGGAAGGT-$(CH_2)'_2$-NH_2-3'.

Instrumentation

The equipment used in this study included a Zimmer Peacock potentiostat using PSTrace 5.8 software, UV-VIS Spectrophotometer (Thermo scientific), Screen Printed Carbon Electrode (SPCE) (GSI Technologies, USA), micropipette (Eppendorf), micro tube, micropipette tip, autoclave sterilizer (Hirayama).

Autoclave HVE-50), scanning electron microscope (Hitachi TM3000) used to characterize the morphology of the electrodes, as well as other general glassware available at the Research Center for Biotechnology and Bioinformatics, Universitas Padjadjaran.

Procedure

Preparation of solution AuNP on 0.76 mM

A 628.53 µL of $HAuCl_4 \cdot 3H_2O$ 55.85 mM and 19.371.47 µL of aqua pro injection were added into the Erlenmeyer flask, followed by stirring with a magnetic stirrer and heating until boiling. Then, 1.730 µL of $Na_3C_6H_5O_7 \cdot 2H_2O$ 1% were added and stirred until the color changed to red wine.

Modified SPCE preparation

The modification was performed by dripping 40 µL of colloidal AuNP solution on the SPCE surface, then allowed to dry for 24 h and rinsed with demineralized water [28]. SPCE before and after modification was characterized using DPV with a 10 mM $K_3[Fe(CN)_6]$ redox system in 0.1 M KCl at a potential range of -1 to +0.7 V and a scan rate of 0.008 V/s, E_{step} 0.004 V with E_{pulse} 0.025 V and t_{pulse} 0.05 s, EIS with 10 mM $K_3[Fe(CN)_6]$ redox system in 0.1 M KCl as well as a frequency of 0.1 to 106 Hz at 0.01 V anodic peak current potential, followed by characterization using cyclic voltammetry (CV) using 10 mM $K_3[Fe(CN)_6]$ in 0.1 M KCl with a scan rate of 0.005 V/s in a potential range of -0.6 V to +0.6 V, and SEM.

Aptamer immobilization on SPCE/AuNP surface

The disulfide bond reduction of the F1 fragment was performed by making an aliquot of 20 µL from F1 4 µM with 5 µL TCEP 0.5 mM, then incubated in the dark for 1 h. Furthermore, it was self-assembled on the SPCE/AuNP surface by dripping 15 µL of aliquot solution and 12 µL of 2 M magnesium chloride for 24 h. The electrode was then rinsed thoroughly with a phosphate buffer solution of pH 7 [29]. The electrodes that have been immobilized with aptamer F1 were characterized using DPV with 10 mM $K_3[Fe(CN)_6]$ redox system in 0.1 M KCl at a potential range of -1 to +0.7 V, the scan rate of 0.008 V/s, E_{step} of 0.004 V with an E_{pulse} of 0.025 V and a t_{pulse} of 0.05 s.

Monitoring of aptasensor response to ATP

A total of 15 µL of ATP with a certain concentration and 15 µL of F2 4 µM were simultaneously dropped on the electrodes and then incubated for various time variations. Furthermore, the modified electrodes were rinsed with a PBS solution of pH 7, making them ready for electrochemical detection [26]. Finally, the electrodes were characterized using DPV with a 10 mM $K_3[Fe(CN)_6]$ redox system in 0.1 M KCl at a potential range of -1 V to +0.7 V, the scan rate of 0.008 V/s, E_{step} of 0.004 V with E_{pulse} of 0.025 V and t_{pulse} of 0.05 s.

Optimization of factors affecting experiments

The factors to be optimized in the experiment includes aptamer F1 concentration (X1), aptamer F2 concentration (X2), and F1/F2/ATP incubation time (X3). Each of these factors is designed using 3 different levels, namely the lowest level (-1), medium (0), and the highest (+1), as shown in Table 1.

Determination of analytical parameters

Creation of calibration curves as well as detection and quantification limits. ATP solutions of various concentrations (0, 0.1, 1, 10, 100, 500, 1000, 2000, 3000) µM were tested on the aptasensor. The resulting electrochemical response was measured using DPV with a 10 mM $K_3[Fe(CN)_6]$ redox system in 0.1 M KCl at a potential range of -1 to +0.7 V and a scan rate of 0.008 V/s, E_{step} of 0.004 V with E_{pulse} of 0.025 V and t_{pulse} of 0.05 s. Furthermore, a curve is made between the concentration and the average peak current difference (ΔI) for each

Table 1. Factor and level of the analysis of experimental condition optimization

Factor	Unit	Level		
		-1	0	+1
Aptamer F1 concentration (X1)	µM	2	4	6
Aptamer F1 incubation time (X2)	hour	6	15	24
F1/F2/ATP incubation time (X3)	minute	2.5	5	7.5

resulting measurement as x and y. Hence, the resulting equation is y = bx + a. The detection and quantification limits are determined using the following equation y = yB + 3SB and y = yB + 10SB, respectively. Where yB is the response to the blank signal, SB is the blank standard deviation, and b is the slope of the regression equation y = a + bx [30].

Determination of precision and accuracy. Precision and accuracy were determined by measuring the ATP solution five times using the previously described procedure. Also, the average difference in peak current (ΔI) and the standard deviation are obtained based on the measurement results. Where $\bar{x}$ is the average measured concentration, and μ is the actual concentration. Meanwhile, the precision is expressed in terms of the coefficient of variance (KV) with the following equation [31].

$$KV = \frac{Sb}{\bar{x}} 100\%$$

$$\text{Precision} = 100\% - KV$$

Meanwhile, accuracy is expressed in percent relative error (%Error) with the following equation [28].

$$\%\text{Error} = \frac{\bar{x} - \mu}{\mu} 100\%$$

$$\text{Accuration} = 100\% - \%\text{Error}$$

Electrochemical aptasensor selectivity test for ATP

On the electrochemical aptasensor that had been designed, the selectivity test was performed by comparing the ATP analyte solution to various nucleotide analogs, such as UTP, CTP, and GTP, each at a concentration of 3000 M. The resulting electrochemical response was measured using DPV with a 10 mM $K_3[Fe(CN)_6]$ redox system in 0.1 M KCl over a potential range of -1 to +0.7 V, the scan rate of 0.008 V/s, E_{step} of 0.004 V with E_{pulse} of 0.025 V and t_{pulse} of 0.05 s.

■ RESULTS AND DISCUSSION

Modification and Characterization of SPCE/AuNP

SPCE Modification with AuNP

The metal nanoparticles exhibit unique physical and chemical properties, different from the bulk or atomic state due to the quantum size effect that produces specific electronic structures. AuNP is one of the most outstanding groups of metal nanoparticles that have attracted considerable interest by promoting various applications in biomedical fields such as biosensing, imaging, and drug delivery systems [32-33].

A UV-Vis spectrophotometer was used to identify the AuNP formation by observing the maximum wavelength value produced. Furthermore, this was indicated by the maximum wavelength on AuNP absorption at 520–530 nm [34]. The nanoparticle size influences the maximum wavelength shift [35]. The AuNP colloid used in this research has an absorption peak at a maximum wavelength of 522, implying that the size used is quite good, as shown in Fig. 1.

Electrochemical biosensors fabricated by combining biological recognition elements with electrochemical transducers modified with AuNPs have become increasingly essential in biosensor research since AuNPs provide a stable surface for the immobilization of biomolecules while retaining their biological activity. However, this is particularly useful when assembling biosensors [36]. This indicates SPCE modification with AuNP was performed to increase the sensitivity. Generally, the achievable sensitivity of an electrochemical detection scheme depends on the amount of electric charge assigned by the label or electrode. This detection sensitivity is increased by modifying the SPCE, which improves the signal element. The modification was made with gold nanomaterials because AuNPs aid in establishing an interface for direct electron transfer from redox-active probes while maintaining their bioactivity. Meanwhile, AuNP increases

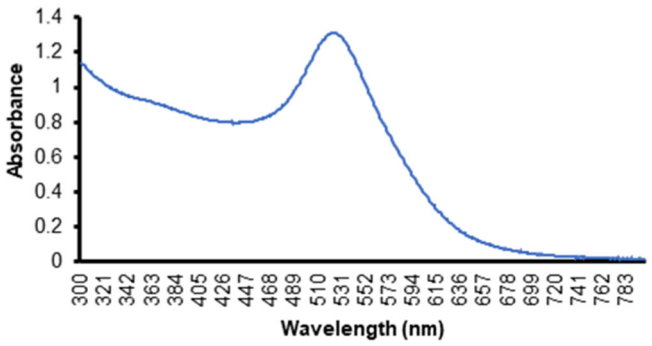

Fig 1. Characterization results of AuNP using UV/Vis spectrophotometer with the maximum wavelength of AuNP absorption at 522 nm

the sensitivity of SPCE with a relatively large surface area and high conductivity.

The modification of SPCE was conducted by dripping 40 AuNP on the surface, then was incubated for 24 h at room temperature to dry. This process takes longer because the physical adsorption method modifies AuNP on the SPCE surface.

SPCE/AuNP Characterization with Differential Pulse Voltammetry

The characterization by differential pulse voltammetry (DPV) was conducted to determine the current response in SPCE before and after modification with AuNP. Furthermore, the electrochemical measurements were performed by observing the oxidation-reduction activity of the electroactive species $[Fe(CN)_6]^{3-/4-}$. The following is an oxidation-reduction reaction in $K_3[Fe(CN)_6]$.

$[Fe(CN)_3]^{3-} + e^- \rightarrow [Fe(CN)_3]^{3-}$

$[Fe(CN)_3]^{4-} \rightarrow [Fe(CN)_3]^{3-} + e^-$

When an analyte is oxidized at the working electrode, current passes electrons to the auxiliary through the external electrical circuit, resulting in solvent reduction.

Fig. 2(a) shows the differential pulse voltammogram of the bare SPCE and AuNP modified SPCE. This shows an increase in peak current in the gold-modified SPCE of 30.979 µA compared to the bare SPCE of 11.133 µA. Furthermore, it implies that the modification provides an electrode surface with increased conductivity. Therefore, the electron transfer between the analyte and the electrode is increased. Fig. 2(b) shows the cyclic voltammogram of the bare SPCE and AuNP modified SPCE; this shows an increase in the redox peak current is associated with an increase in electrochemical activity with an increase in the active electrode area.

SPCE/AuNP Characterization by Electrochemical Impedance Spectroscopy

The characterization by electrochemical impedance spectroscopy (EIS) was conducted on SPCE before and after modification with AuNP, where the measurement was based on impedance or resistance. Fig. 3 shows the characterization results of the bare SPCE and

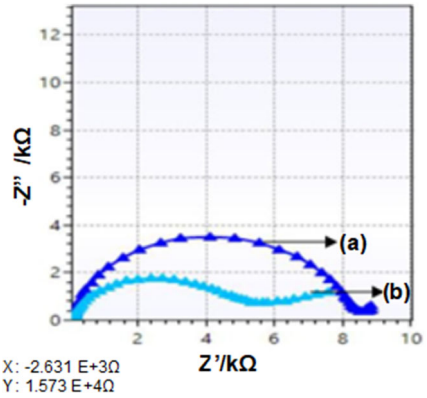

Fig 2. SPCE characterization result spectrum using EIS; line (a) Bare SPCE and line (b) SPCE/AuNP using a redox system of 10 mM potassium ferricyanide $K_3[Fe(CN)_6]$ solution in 0.1 M KCl at a frequency of 0.1 to 10^6 Hz at an anodic peak current potential of 0.01 V

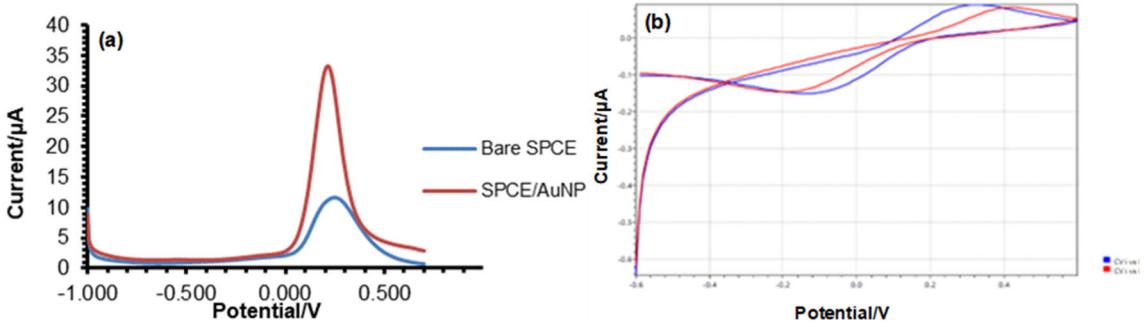

Fig 3. (a) Differential pulse voltammogram: bare SPCE (blue line) and SPCE/AuNP (red line) with 10 mM $K_3[Fe(CN)_6]$ redox system in 0.1 M KCl solution. The scan rate of 0.008 V/s was used in the potential range of -1.0 to +0.7 V. (b) Cyclic voltammograms: bare SPCE (red line) and SPCE/AuNP (blue line) with 10 mM $K_3[Fe(CN)_6]$ in 0.1 M KCl with a scan rate of 0.005 V/s over a potential range of -0.6 V to +0.6 V

AuNP-modified SPCE using EIS. The gold-modified SPCE showed a decrease when compared to the bare SPCE. The characterization results using EIS are inversely proportional to DPV because resistance and current are inversely proportional to Ohm's Law, namely V = I. R. This shows that the modification of SPCE with AuNP provides an electrode surface with increased conductivity. Therefore, there is an increase in the electron transfer between the analyte-electrodes, and the impedance value becomes lower. The measurement of the circle diameter (Rct) in the circular section of the Nyquist plot is related to the high frequency of the electron transfer process as opposed to the electron transfer current, which shows the results of surface modification of SPCE with AuNP. In Fig. 3 (line a), the unmodified SPCE has a large Rct due to the current decrease in the electron transfer process, so the resistance obtained is very large. The Rct of the gold-modified SPCE surface (line b) was smaller than that of the unmodified electrode (line a). After modification of the SPCE surface, the current increases so that the resistance is obtained, as shown in line b.

SPCE/AuNP Surface Characterization using Scanning Electron Microscopy (SEM)

SEM was used to examine the morphology of gold nanoparticles, which involves scanning the sample surface for particle shape using a high-energy radiance. Fig. 4 shows the surface morphology of SPCE before and after being modified with SEM gold nanoparticles, with a and b showing the SPCE surface before and after being modified with AuNP, respectively. Since AuNP has adhered to the SPCE surface after being changed, the final surface is more closed, thereby implying that the modification has been completed successfully.

Aptamer F1 Immobilization on Electrode Surface

Characterization of SPCE/AuNP/F1 with differential pulse voltammetry

The differential pulse voltammetry (DPV) based on electron transfer from $K_3[Fe(CN)_6]$ as the electroactive species experiencing a redox reaction was used to determine the success of aptamer F1 immobilization in SPCE/AuNP. There is a decrease in peak current due to the aptamer F1 on the electrode surface. The results of the DPV voltammogram before and after the immobilization of the aptamer F1 are shown in Fig. 5.

After the aptamer F1 was immobilized on the SPCE surface, there was a decrease in the peak current on the DPV voltammogram to 22.619 μA. This shows that the immobilization has been conducted successfully because compounds on the SPCE surface will disrupt the electron transfer between the redox probe and the electrode.

AuNPs are particularly suitable for diagnostics because they are easily modified with thiolated ligands to detect specific molecules of interest [32]. The immobilization technique of the aptamer F1, which has modified the thiol group on SPCE/AuNP through covalent bonds, shows good stability, flexibility, and high binding strength. This procedure results in the specific binding of the aptamer to the electrode surface

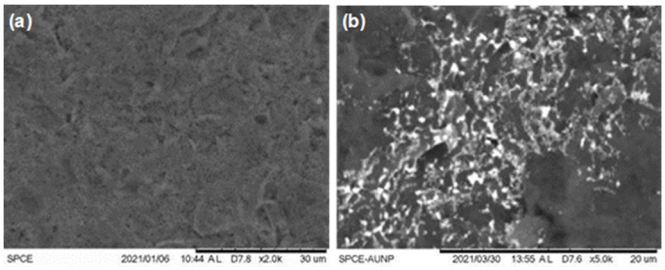

Fig 4. Characterization results of modified SPACE using SEM; (a) SPCE bare, (b) SPCE/AuNP

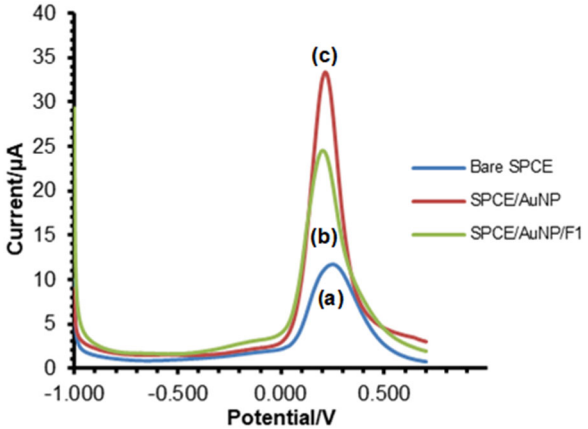

Fig 5. Differential pulse voltammogram: (a) bare SPCE, (b) SPCE/AuNP, (c) SPCE/AuNP/F1 with 10 mM $K_3[Fe(CN)_6]$ redox system in 0.1 M KCl solution. The scan rate of 0.008 V/s was used in the potential range of -1.0 V to +0.7 V

and prevents non-specific binding. Furthermore, the immobilization occurs covalently between the thiol-modified aptamer and the surface of AuNP to form a self-assembled monolayer due to the strong affinity interaction between the thiol group and the gold surface, forming an Au-SH covalent bond.

SPCE/AuNP/F1 surface characterization using scanning electron microscopy (SEM)

The efficacy of the aptamer F1 immobilization on SPCE/AuNP was tested using SEM. The characterization result of SPCE/AuNP/F1 is shown in Fig. 6, where the electrode surface is covered with a triangular shape aptamer. This implies that the immobilization of the aptamer F1 on the SPCE/AuNP surface has been conducted successfully.

Aptasensor testing on ATP and its characterization

The aptasensor test was conducted by dripping each 15 µL of aptamers F2 and ATP simultaneously on the SPCE/AuNP/F1 surface and incubated for 7.5 min at room temperature. Furthermore, the aptasensors were washed with a pH 7 PBS solution to remove nonadherent species from the SPCE/AuNP/F1 surface. Hence, it reduces errors while measuring currents that interfere with the analysis process. After adding the aptamer F2 and ATP on the SPCE/AuNP/F1 surface, there will be an association between F2 and F1 in the presence of ATP, forming a sandwich/g-quadruplex structure on the AuNP surface. The illustration of this aptasensor is shown in Fig. 7.

The aptamer layer on the electrode surface gets denser due to the association between F1 and F2, and the negative charge increases more than in the previous stage. Therefore, negatively charged ferricyanide ions will be inhibited from approaching the electrode, reducing electron transmission between the redox probe and the electrode. The current decreased to 16.775 mA, as shown in Fig. 8.

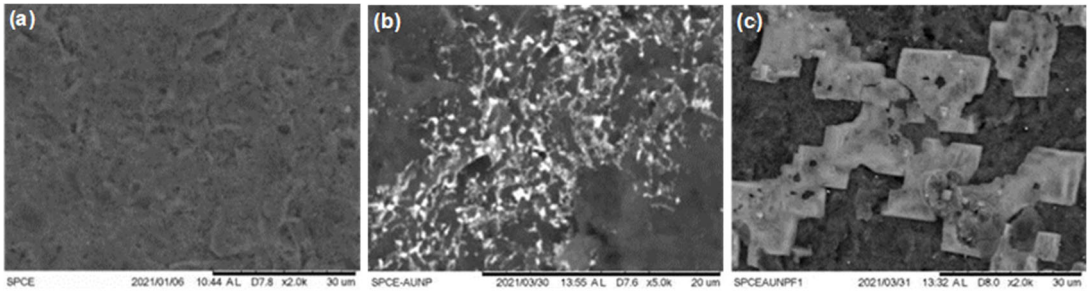

Fig 6. Characterization results of modified SPACE using SEM; (a) bare SPCE, (b) SPCE/AuNP, and (c) SPCE/AuNP/F1

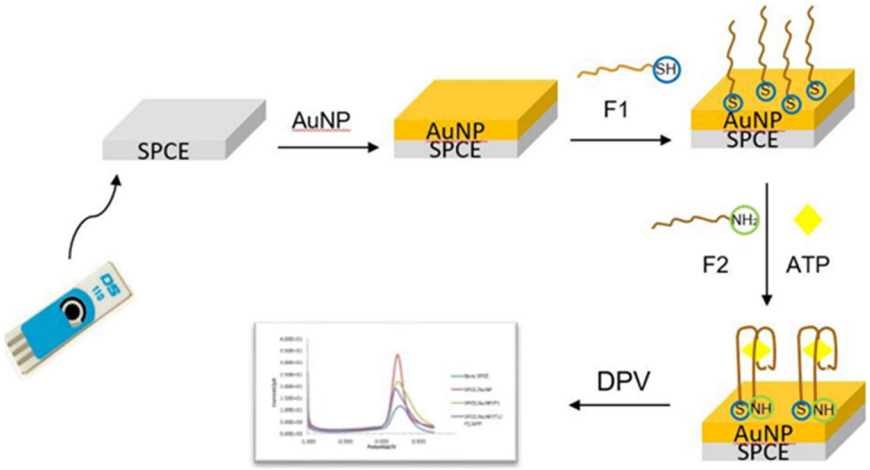

Fig 7. Illustration of an aptamer-based electrochemical biosensor for detecting ATP using APCE/AuNP

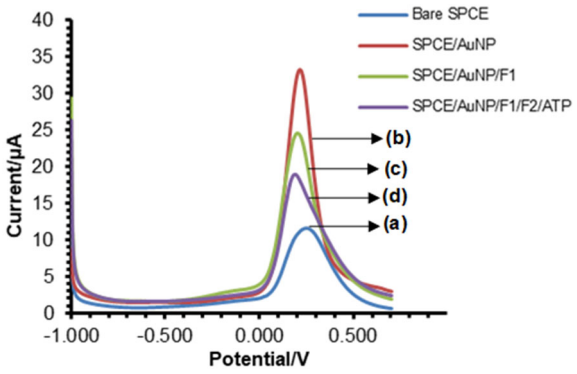

Fig 8. Differential pulse voltammogram: (a) bare SPCE, (b) SPCE/AuNP, (c) SPCE/AuNP-F1, (d) SPCE/AuNP-F1-F2-ATP with 10 mM $K_3[Fe(CN)_6]$ redox system in 0.1 M KCl solution. The scan rate of 0.008 V/s is used in the potential range of -1.0 V to +0 .7 V

Determination of Optimum Conditions with Box-Behnken Experiment Design

The factors optimized in the experiment include aptamer F1 concentration (X1), aptamer F2 concentration (X2), and F1/F2/ATP incubation time (X3). Furthermore, each of them is designed through 3 different levels, namely, the lowest level (-1), medium (0), and the highest (+1). Three experimental factors, each with three levels, produced 15 trials and were divided into two replication blocks for two repeats, yielding a total of 30 trials with the outcome in the form of current response (A), as shown in Table 2.

The response of the measurement results is processed with the Minitab 18 prog, and the coefficients

Table 2. Factor, level, and current response in the optimization analysis of experimental conditions

No.	Aptamer F1 concentration (µM)	Aptamer F1 incubation time (h)	F1/F2/ATP incubation time (min)	Current response (µA)
1	2	6	5.0	20.902
2	6	6	5.0	18.078
3	2	24	5.0	17.852
4	6	24	5.0	17.794
5	2	15	2.5	20.877
6	6	15	2.5	21.860
7	2	15	7.5	20.282
8	6	15	7.5	16.663
9	4	6	2.5	15.134
10	4	24	2.5	15.657
11	4	6	7.5	21.033
12	4	24	7.5	13.145
13	4	15	5.0	15.392
14	4	15	5.0	13.924
15	4	15	5.0	15.392
16	2	6	5.0	20.546
17	6	6	5.0	21.743
18	2	24	5.0	17.852
19	6	24	5.0	17.704
20	2	15	2.5	20.887
21	6	15	2.5	14.184
22	2	15	7.5	16.640
23	6	15	7.5	14.609
24	4	6	2.5	16.134
25	4	24	2.5	14.296
26	4	6	7.5	21.033
27	4	24	7.5	12.902
28	4	15	5.0	17.294
29	4	15	5.0	14.962
30	4	15	5.0	17.627

Table 3. P-value of ANOVA results for each factor

Factor	P-Value
Aptamer F1 concentration	0.120
Aptamer F1 incubation time	0.003
F1/F2/ATP incubation time	0.741

and response functions are obtained to determine the maximum current. Furthermore, this method is an experimental design using statistics and mathematics to discover the optimal value. Based on the results of the ANOVA output, the most significant factor affecting the experiment was the aptamer F1 incubation time because it had a P-value < 0.05, as shown in Table 2. The current response obtained is then analyzed, showing the coefficient of the response function in Eq. (1).

$$Y = 26.73 - 5.95X1 - 0.045X2 + 1.48X3 + 0.672X1^2 + 0.00747X2^2 - 0.033X3^2 + 0.0099X1 * X2 + 0.002X1 * X3 - 0.081X2 * X3 \quad (1)$$

X1: Aptamer F1 concentration, X2: Aptamer F1 incubation time, X3: F1/F2/ATP incubation time.

In the experiment, the component with negative value effects decreases the reaction, while the factor with a positive value increases the response, as shown in Eq. (1). The optimum conditions obtained from the results of the Box-Behnken experimental design for each factor include the aptamer F1 concentration of 4 µM, aptamer F1 incubation time of 24 h, and the F1/F2/ATP incubation time of 7.5 min.

Calibration Curves, Detection Limits, and Quantification Limits

A calibration curve is drawn after determining the optimum conditions of several factors that affect the experiment. Also, the detection and quantification limits of this electrochemical aptasensor are calculated using variations in ATP concentration. The experiment was conducted similarly to the procedure for determining the aptasensor response by using the parameters of the optimization results. ATP with various concentrations (0; 0.1; 1; 10; 100) µM was tested on an electrochemical aptasensor to describe the amount present in the sample and measured twice at each concentration. The resulting electrochemical response using DPV is shown in Fig. 9.

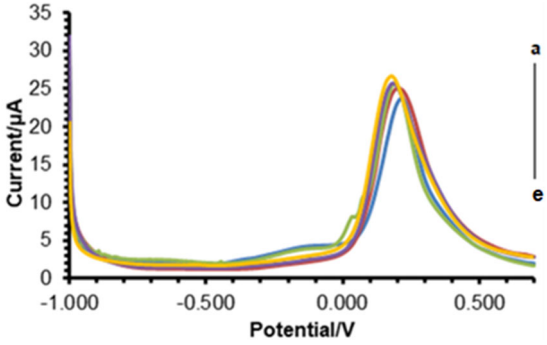

Fig 9. Differential pulse voltammogram for variations in ATP concentration a–e (0, 0.1, 1, 10, 100) µM as measured by a 10 mM $K_3[Fe(CN)_6]$ solution redox system in 0.1 M KCl solution with a scan rate of 0.008 V/s over a potential range of -1.0 V to +0.7 V, E_{step} of 0.004 V with E_{pulse} of 0.025 V and t_{pulse} of 0.05 s

Based on the characterization results using the DPV, it is known that the higher the concentration of ATP added, the lower the peak value of the current generated. As a result, the aptamer binds, crowding the SPCE surface and interrupting electron transport between the potassium ferricyanide redox probe and the electrode. A calibration curve was made by plotting the peak value of the DPV current as a result of the characterization of ATP concentration variations with concentration variations (0.1; 1; 10; 100) µM, as shown in Fig. 10. From the calibration curve, the linear regression equation y = 0.0124x + 0.8769 is obtained with R^2 of 0.9952. Based on the data processing results, the value of the detection (LoD) and quantification (LoQ) limits is 7.43 and 24.78 µM, then the accuracy and precision values are 96 and 98.69%, respectively.

The detection limit obtained on the aptasensor for ATP detection in this research is quite good compared to Zheng et al. [20], which was carried out using a conventional 3 electrode system, and Ren et al. [37] used a fluorescence aptasensor. Hence, the electrochemical aptasensor method using SPCE/AuNP is superior in sensitivity and stability. However, the detection limit is still higher when compared to Mashhadizadeh et al., that used silver nanoparticle modified graphene oxide (AgNP) nanocomposites, where graphene oxide as a substrate for binding large amounts of AgNP enhances

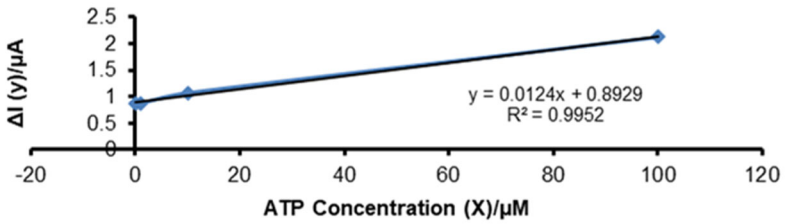

Fig 10. ATP aptasensor calibration curve with variations in concentration (0.1; 1; 10; 100) μM as measured by a of 10 mM $K_3[Fe(CN)_6]$ solution redox system in 0.1 M KCl. The scan rate is at 0.008 V/s over a potential range of -1.0 V to +0.7 V, E_{step} of 0.004 V with an E_{pulse} of 0.025 V and a t_{pulse} of 0.05 s

Table 4. Research on aptamer-based biosensors to detect ATP

	LoD	Ref.
Label-free fluorescence aptasensor based on AuNPs and CQDs for the detection of ATP	20 μM	[37]
Electrochemical nanoaptasensor for continuous monitoring ATP fluctuation at subcellular level	26 μM	[20]
Aptamer-based electrochemical biosensor for detecting Adenosine Triphosphate (ATP) using Screen Printed Carbon Electrode/Gold Nanoparticles (SPCE/AuNP)	7.43 μM	This research
A simple non-enzymatic strategy for adenosine triphosphate electrochemical aptasensor using silver nanoparticle-decorated graphene oxide	5.0 nM	[19]
A sensitive colorimetric aptasensor with a triple-helix molecular switch based on peroxidase-like	2.4 nM	[38]

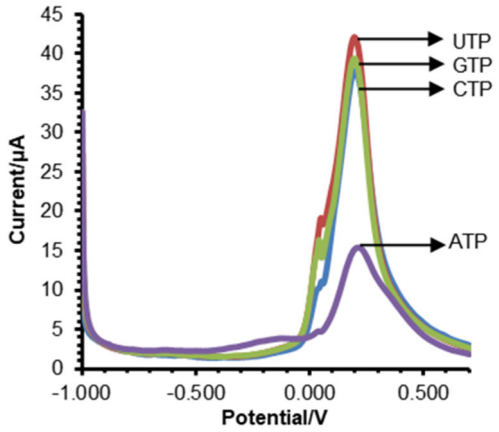

Fig 11. Electrochemical aptasensor response voltammogram for ATP in detecting ATP, UTP, GTP, and CTP at a concentration of 3 μM as measured by a 10 mM $K_3[Fe(CN)_6]$ solution redox system in 0.1 M KCl solution. The scan rate is at 0.008 V/s over a potential range of -1.0 V to +0.7 V, E_{step} of 0.004 V with E_{pulse} of 0.025 V and tp_{ulse} of 0.05 s

the amplification AgNP oxidation signals [19]. Shahsavar et al. used a colorimetric biosensor with DNAzyme [38], as shown in Table 4.

Electrochemical Aptasensor Selectivity for ATP

The selectivity of this electrochemical aptasensor for ATP was investigated by determining the current response when the sensor was added to other nucleotide analogue analytes, which include UTP, GTP, and CTP.

The result of the voltammogram characterization in Fig. 11 shows that the peak current in ATP is 12.455 μA, while UTP, CTP, and GTP produce higher current peaks than ATP at 39.934, 35.446, and 37.034 μA, respectively. The peak DPV current in the ATP analog increases as in the analyte without ATP. Therefore, it can be seen that this electrochemical aptasensor shows a selective response to ATP.

■ CONCLUSION

The aptamer was successfully mobilized on the surface of the SPCE modified gold nanoparticles with the characterization results using differential pulse voltammetry, where the current decreased from 30.979

to 22.619 µA. Based on the results of SEM characterization, it is shown that the SPCE surface has been covered by aptamers. The optimum conditions obtained through the Box-Behnken experimental design were ATP concentration of 4 µM, aptamer F1 incubation time for 24 h, and F1/F2/ATP incubation time for 7.5 min. Therefore, the detection and quantification (LoD) and limits (LoQ) of the electrochemical aptasensors for ATP developed in this research were 7.43 and 24.78 µM, respectively.

■ ACKNOWLEDGMENTS

The authors are grateful for the financial support from the second-year doctoral funding grant of the Indonesian Ministry of Research, Technology and Higher Education, Number: 1827/UN6.3.1/LT/2020, Academic Leadership Grant (ALG) DRPMI Universitas Padjadjaran, Number: 1427/UN6.3.1/LT/2020 and national competitive basic research funding grand of the Indonesian Ministry of Research, Technology and Higher Education, Number: 094/E5/PG.02.00.PT/2022.

■ AUTHOR CONTRIBUTIONS

Rahmaniar Mulyani and Nida Yumna conducted the experiment, Nida Yumna conducted the calculations optimization Box-Behnken design, Rahmaniar Mulyani, Iman Permana Maksum, and Yeni Wahyuni Hartati wrote and revised the manuscript. Toto Subroto revised the manuscript. All authors agreed to the final version of this manuscript.

■ REFERENCES

[1] Huang, Y., Lei, J., Cheng, Y., and Ju, H., 2015, Target-assistant Zn^{2+}-dependent DNAzyme for signal-on electrochemiluminescent biosensing, *Electrochim. Acta*, 155, 341–347.

[2] Frazier, A.E., Thorburn, D.R., and Compton, A.G., 2019, Mitochondrial energy generation disorders: Genes, mechanisms, and clues to pathology, *J. Biol. Chem.*, 294 (14), 5386–5395.

[3] Maksum, I.P., Farhani, A., Rachman, S.D., and Ngili, Y., 2013, Making of the A3243G mutant template through site directed mutagenesis as positive control in PASA-Mismatch three bases, *Int. J. PharmTech Res.*, 5 (2), 441–450.

[4] Maksum, I.P., Natradisastra, G., Nuswantara, S., and Ngili, Y., 2013, The effect of A3243G mutation of mitochondrial DNA to the clinical features of type-2 diabetes mellitus and cataract, *Eur. J. Sci. Res.*, 96 (4), 591–599.

[5] Hartati, Y.W., Nur Topkaya, S., Maksum, I.P., and Ozsoz, M., 2013, Sensitive detection of mitochondrial DNA A3243G tRNALeu mutation via an electrochemical biosensor using Meldola's Blue as a hybridization indicator, *Adv. Anal. Chem.*, 3 (A), 20–27.

[6] Destiarani, W., Mulyani, R., Yusuf, M., and Maksum, I.P., 2020, Molecular dynamics simulation of T10609C and C10676G mutations of mitochondrial *ND4L* gene associated with proton translocation in type 2 diabetes mellitus and cataract patients, *Bioinf. Biol. Insights*, 14, 117793222097867.

[7] Maksum, I.P., Saputra, S.R., Indrayati, N., Yusuf, M., and Subroto, T., 2017, Bioinformatics study of m.9053G>A mutation at the *ATP6* gene in relation to type 2 diabetes mellitus and cataract diseases, *Bioinf. Biol. Insights*, 11, 1177932217728515.

[8] Ning, Y., Wei, K., Cheng, L., Hu, J., and Xiang, Q., 2017, Fluorometric aptamer based determination of adenosine triphosphate based on deoxyribonuclease I-aided target recycling and signal amplification using graphene oxide as a quencher, *Microchim. Acta*, 184 (6), 1847–1854.

[9] Qu, F., Sun, C., Lv, X., and You, J., 2018, A terbium-based metal-organic framework@gold nanoparticle system as a fluorometric probe for aptamer based determination of adenosine triphosphate, *Microchim. Acta*, 185 (8), 359.

[10] Liu, X., Lin, B., Yu, Y., Cao, Y., and Guo, M., 2018, A multifunctional probe based on the use of labeled aptamer and magnetic nanoparticles for fluorometric determination of adenosine 5'-triphosphate, *Microchim. Acta*, 185 (4), 243.

[11] Khlyntseva, S.V., Bazel', Y.R., Vishnikin, A.B., and Andruch, V., 2009, Methods for the determination of adenosine triphosphate and other adenine nucleotides, *J. Anal. Chem.*, 64 (7), 657–673.

[12] Huang, Y.F., and Chang, H.T., 2007, Analysis of adenosine triphosphate and glutathione through gold nanoparticles assisted laser desorption/ionization mass spectrometry, *Anal. Chem.*, 79 (13), 4852–4859.

[13] Srivastava, P., Razi, S.S., Ali, R., Srivastav, S., Patnaik, S., Srikrishna, S., and Misra, A., 2015, Highly sensitive cell imaging "Off–On" fluorescent probe for mitochondria and ATP, *Biosens. Bioelectron.*, 69, 179–185.

[14] Chen, J.R., Jiao, X.X., Luo, H.Q., and Li, N.B., 2013, Probe-label-free electrochemical aptasensor based on methylene blue-anchored graphene oxide amplification, *J. Mater. Chem. B*, 1 (6), 861–864.

[15] Yi, Q., and Yu, W., 2009, Nanoporous gold particles modified titanium electrode for hydrazine oxidation, *J. Electroanal. Chem.*, 633 (1), 159–164.

[16] Yáñez-Sedeño, P., Villalonga, R., and Pingarrón, J.M., 2015, "Electroanalytical Methods Based on Hybrid Nanomaterials" in *Encyclopedia of Analytical Chemistry*, John Wiley & Sons, Ltd, Chichester, UK, 1–18.

[17] Goud, K.Y., Moonla, C., Mishra, R.K., Yu, C., Narayan, R., Litvan, I., and Wang, J., 2019, Wearable electrochemical microneedle sensor for continuous monitoring of levodopa: Toward Parkinson management, *ACS Sens.*, 4 (8), 2196–2204.

[18] Villalonga, A., Pérez-Calabuig, A.M., and Villalonga, R., 2020, Electrochemical biosensors based on nucleic acid aptamers, *Anal. Bioanal. Chem.*, 412 (1), 55–72.

[19] Mashhadizadeh, M.H., Naseri, N., and Mehrgardi, M.A., 2017, A simple non-enzymatic strategy for adenosine triphosphate electrochemical aptasensor using silver nanoparticle-decorated graphene oxide, *J. Iran. Chem. Soc.*, 14 (9), 2007–2016.

[20] Zheng, J., Li, X., Wang, K., Song, J., and Qi, H., 2020, Electrochemical nanoaptasensor for continuous monitoring of ATP fluctuation at subcellular level, *Anal. Chem.*, 92 (16), 10940–10945.

[21] Metters, J.P., Kadara, R.O., and Banks, C.E., 2011, New directions in screen printed electroanalytical sensors: An overview of recent developments, *Analyst*, 136 (6), 1067.

[22] Mulyasuryani, A., and Dofir, M., 2014, Enzyme biosensor for detection of organophosphate pesticide residues base on screen printed carbon electrode (SPCE)-bovine serum albumin (BSA), *Engineering*, 6 (5), 230–235.

[23] Taleat, Z., Khoshroo, A., and Mazloum-Ardakani, M., 2014, Screen-printed electrodes for biosensing: A review (2008–2013), *Microchim. Acta*, 181 (9), 865–891.

[24] Dorledo de Faria, R.A., Messaddeq, Y., Heneine, G.D., and Matencio, T., 2019, Application of screen-printed carbon electrode as an electrochemical transducer in biosensors, *Int. J. Biosens. Bioelectron.*, 5 (1), 1–2.

[25] Kanyong, P., Rawlinson, S., and Davis, J., 2016, Gold nanoparticle modified screen-printed carbon arrays for the simultaneous electrochemical analysis of lead and copper in tap water, *Microchim. Acta*, 183 (8), 2361–2368.

[26] Dridi, F., Marrakchi, M., Gargouri, M., Saulnier, J., Jaffrezic-Renault, N., and Lagarde, F., 2017, "Nanomaterial-Based Electrochemical Biosensors for Food Safety and Quality Assessment" in *Nanobiosensors*, Eds. Grumezescu, A.M., Academic Press, Cambridge, US, 167–204.

[27] Zhao, X., Mai, Z., Kang, X., and Zou, X., 2008, Direct electrochemistry and electrocatalysis of horseradish peroxidase based on clay–chitosan-gold nanoparticle nanocomposite, *Biosens. Bioelectron.*, 23 (7), 1032–1038.

[28] Bernardo-Boongaling, V.R.R., Serrano, N., García-Guzmán, J.J., Palacios-Santander, J.M., and Díaz-Cruz, J.M., 2019, Screen-printed electrodes modified with green-synthesized gold nanoparticles for the electrochemical determination of aminothiols, *J. Electroanal. Chem.*, 847, 113184.

[29] Kashefi-Kheyrabadi, L., and Mehrgardi, M.A., 2013, Aptamer-based electrochemical biosensor for detection of adenosine triphosphate using a

nanoporous gold platform, *Bioelectrochemistry*, 94, 47–52.

[30] Miller, J.N., 1991, Basic statistical methods for analytical chemistry. Part 2. Calibration and regression methods, A review, *Analyst*, 116 (1), 3–14.

[31] Skoog, D.A., Holler, F.J., and Nieman, T.A., 1998, *Principles of Instrumental Analysis*, 5th Ed., Saunders College Publishing, Philadelphia, US.

[32] Hwu, S., Garzuel, M., Forró, C., Ihle, S.J., Reichmuth, A.M., Kurdzesau, F., and Vörös, J., 2020, An analytical method to control the surface density and stability of DNA-gold nanoparticles for an optimized biosensor, *Colloids Surf., B*, 187, 110650.

[33] Zhao, P., Li, N., and Astruc, D., 2013, State of the art in gold nanoparticle synthesis, *Coord. Chem. Rev.*, 257 (3-4), 638–665.

[34] Apyari, V.V., Arkhipova, V.V., Dmitrienko, S.G., and Zolotov, Y.A., 2014, Using gold nanoparticles in spectrophotometry, *J. Anal. Chem.*, 69 (1), 1–11.

[35] Fatimah, S., Haryati, I., and Jamaludin, A., 2009, Pengaruh Uranium terhadap Analisis Thorium menggunakan Spektrofotometer UV-Vis, *Seminar Nasional V SDM Teknologi Nuklir*, 5 November 2009, Yogyakarta, 573–578.

[36] Yáñez-Sedeño, P., and Pingarrón, J.M., 2005, Gold nanoparticle-based electrochemical biosensors, *Anal. Bioanal. Chem.*, 382 (4), 884–886.

[37] Ren, L., Xu, P., Zhang, P., Qin, Z., Zhang, Y., and Jiang, L., 2021, Label-free fluorescence aptasensor based on AuNPs and CQDs for the detection of ATP, *AIP Adv.*, 11, 015316.

[38] Shahsavar, K., Hosseini, M., Shokri, E., Ganjali, M.R., and Ju, H., 2017, A sensitive colorimetric aptasensor with a triple-helix molecular switch based on peroxidase-like activity of a DNAzyme for ATP detection, *Anal. Methods*, 9 (32), 4726–4731.